1 **Impacts of tropical cyclone-heatwave compound events on surface ozone in eastern**

2 **China: Comparison between the Yangtze River and Pearl River Deltas**

3

4 Cuini Qi [1], Pinya Wang [1, *], Yang Yang [1, *], Huimin Li [1], Hui Zhang [1], Lili Ren [2], Xipeng Jin [1],

5 Chenchao Zhan [3], Jianping Tang [4], Hong Liao [1]

6 [1]Jiangsu Key Laboratory of Atmospheric Environment Monitoring and Pollution Control,

7 Jiangsu Collaborative Innovation Center of Atmospheric Environment and Equipment

8 Technology, Joint International Research Laboratory of Climate and Environment Change, School

9 of Environmental Science and Engineering, Nanjing University of Information Science and

10 Technology, Nanjing, Jiangsu, China

11 [2]College of Environment and Ecology, Jiangsu Open University, Nanjing, Jiangsu, China

12 [3]School of Atmospheric Physics, Nanjing University of Information Science and Technology,

13 Nanjing, Jiangsu, China

14 [4]School of Atmospheric Sciences, Nanjing University, Nanjing, Jiangsu, China

15

16

17 Correspondence to: Pinya Wang, pinya.wang@nuist.edu.cn

18 Yang Yang, yang.yang@nuist.edu.cn

19

20 **Abstract**

21   China has implemented some air pollution management measures in recent years, yet severe

22 ozone pollution remains a significant issue. The Southeastern Coast of China (SECC) is often

23 influenced by hot extremes and tropical cyclones (TCs), and the two can occur simultaneously (TC-

24 HDs). The compound TC-HDs show a rising trend in the summers of 2014-2019, potentially

25 affecting ozone pollution. Here, we found that surface ozone concentrations over SECC are more

26 elevated during extreme hot days than the summer climatology. However, compared to extreme hot

27 days alone (AHDs), the maximum 8-hour average ozone (MDA8 O_3) concentration increases by an

28 average of 6.8 $\mu g/m^3$ in the Pearl River Delta (PRD) and decreases by 13.2 $\mu g/m^3$ in the Yangtze

29 River Delta (YRD) during the compound TC-HDs. The meteorological conditions during AHDs

30 favor the chemical production of ozone over SECC, exhibiting increased temperature and solar

31 radiation and decreased relative humidity. Relative to AHDs, strong northeasterly winds prevail in

32 SECC during TC-HDs, suggesting the potential of ozone cross-regional transport between YRD and

33 PRD. The process analysis in the chemical transport model (GEOS-Chem) suggests that relative to

34 AHDs, the chemical production of ozone is enhanced in YRD during TC-HDs while horizontal

35 transport alleviates ozone pollution in YRD but worsens it in PRD through cross-regional transport.

36 The results highlight the significant effects of cross-regional transport in modulating ozone pollution

37 in the two megacity clusters during hot extremes accompanied by TC activities, giving insight into

38 future ozone control measures over SECC under global warming.

39

1. Introduction

Tropospheric ozone (O$_3$) is the predominant air pollutant in addition to fine particulate matter (PM$_{2.5}$) in China (Fu et al., 2019), and it poses significant risks to human health and the ecosystem (Feng et al., 2015; Wang et al., 2017). Long-term exposure to high concentrations of ozone could lead to lung tissue damage and chronic obstructive pulmonary disease, thereby increasing premature death (Turner et al., 2016; Liu et al., 2018). Chen et al. (2023) demonstrated that the deterioration of ozone air quality is considered to be the primary factor responsible for the 90% increase in premature respiratory mortalities in China from 2013 to 2019. Furthermore, ozone can negatively impact crop yield by inhibiting plant photosynthesis, accelerating crop senescence, and reducing both yield and quality (Ainsworth et al., 2012; Song and Hao, 2023), ultimately affecting ecosystem stability (Gu et al., 2023).

To deal with the severe air pollution issues, China has implemented several pollution prevention and control measures, which are prioritized to tackle the problem of particulate matter, including the "Air Pollution Prevention and Control Action Plan" and the "Three-Year Action Plan for Winning the Blue Sky Defense Battle" (P. Wang et al., 2022). These efforts are making significant progress in lowering PM$_{2.5}$ concentrations. Z. Wang et al. (2022) indicated that the annual concentration of PM$_{2.5}$ in China has decreased by 13.41 μg/m^3 from 2014 to 2020. However, it is worth noting that most cities in China still frequently experienced severe ozone episodes (Li et al., 2019). It is demonstrated that surface ozone concentrations in most regions of China have increased by approximately 20% during the period from 2013 to 2017 (Huang et al., 2018). Also, Wei et al. (2022) recently found that both surface ozone concentration and ozone pollution days (the maximum

61   8-hour average ozone (MDA8 O_3) concentrations exceed 160 µg/m³) in China exhibited an

62   increasing trend from 2013 to 2020. Therefore, ozone pollution in China has received widespread

63   attention over the past few decades (Ashmore, 2005; Gong and Liao, 2019; N. Wang et al., 2022).

64   Changes in tropospheric ozone are closely related to their precursor gases, including nitrogen

65   oxides (NO_x) and volatile organic compounds (VOCs) (Fu and Liao, 2014; Jacob et al., 1999; Li et

66   al., 2019). Zhang et al. (2023) revealed that an increase in biogenic volatile organic compounds

67   (BVOCs) increased local ozone production by 23% per year in Hong Kong. Li et al. (2019) pointed

68   out that anthropogenic NO_x emissions in China decreased by 21% from 2013 to 2017, whereas

69   VOCs emissions changed little. Decreasing NO_x would increase ozone under the VOC-limited

70   conditions prevailed in urban China but decrease ozone under rural NO_x-limited conditions. In

71   addition to precursor emissions, meteorological conditions can significantly modulate surface ozone

72   levels (Yin et al., 2019; Zhou et al., 2022). For example, severe ozone pollution commonly occurs

73   during summertime with high temperatures, low relative humidity (RH), and strong solar radiation

74   (Dai et al., 2023; Yin et al., 2019). Under low RH conditions, trees close the stomata (pores for

75   exchanging CO_2 and water vapor), inhibiting the dry deposition of ozone and leading to ozone

76   accumulation (Kavassalis and Murphy, 2017). Besides, low humidity conditions inhibit ozone

77   breakdown as the O(^{1}D) combines with water molecules (H_2O) to produce hydroxyl radicals that

78   promote ozone decomposition in high-humidity environments (M. Li et al., 2021). Wind direction

79   and wind speed play an important role in the transport and diffusion of ozone (Banta et al., 2011;

80   Jammalamadaka and Lund, 2006). It is proved that the co-occurred heat waves and atmospheric

81   stagnation days with low wind speeds favor ozone pollution in the U.S. through promoting the ozone

82 production (Zhang et al., 2018). Reduced clouds and strengthened solar radiation during the hot

83 extremes favor photochemical ozone production in the troposphere and thus increase the surface

84 ozone concentrations (P. Wang et al., 2022). Large-scale atmospheric circulation can modulate

85 surface ozone through changing the meteorological conditions (Yang et al., 2022). For instance, the

86 stronger western Pacific subtropical high (WPSH) leads to higher temperatures, stronger solar

87 radiation, lower RH, and less precipitation, which favors the production and accumulation of surface

88 ozone in northern China (Jiang et al., 2021).

89 Extreme weather events, especially heat waves and tropical cyclones (TCs), have a significant

90 impact on ozone pollution in eastern China (Lin et al., 2019; T. Wang et al., 2017). High ozone

91 concentration events are typically associated with high temperatures, which lead to increased

92 emissions of BVOCs and enhance the chemical formation of ozone (Lu et al., 2019; P. Wang et al.,

93 2022). P. Wang et al. (2022) indicate that ozone pollution levels are significantly higher during

94 extreme heat events compared to other days in the North China Plain. TC activities can substantially

95 affect tropospheric ozone by affecting the chemical production, transport, and accumulation

96 processes over the coastal regions of China (K. Meng et al., 2022; Qu et al., 2021; Zhan et al., 2022).

97 Shu et al (2016) investigated the impacts of Typhoon Utor on an ozone pollution episode over the

98 Yangtze River Delta (YRD) of China from August 7 to 12, 2013. They found that the peripheral

99 circulations of the approaching typhoon intensified downward airflow, leading to a short-term local

100 weather pattern of high temperatures, low humidity, intense solar radiation, and light winds, which

101 exacerbated ozone pollution. Following the passage of TCs, the lower tropospheric transport of

102 ozone-rich air and strong photochemical reactions also contribute to amplifying ozone pollution

103   (Zhan et al., 2020). For ozone pollution in Pearl River Delta (PRD), influenced by the strong

104   downdrafts related to the periphery of TCs, the PRD region typically is dominated by high pressure,

105   low humidity, and strong solar radiation, leading to the accumulation of ozone (Wei et al., 2016;

106   Ouyang et al., 2022). Moreover, TC activities are proven to enhance the chemical interactions

107   between anthropogenic and biogenic emissions, resulting in extreme ozone pollution over both the

108   YRD and PRD regions (N. Wang et al., 2022).

109   The southeastern coastal region of China (SECC), including the YRD and PRD regions,

110   experiences both frequent TCs and heatwave events under global warming (W. Wang et al., 2016;

111   Xiao et al., 2011). And there is a significant concurrent relationship between extreme heatwaves and

112   TC activity that the peripheral circulations of TCs can promote extreme heatwaves (P. Wang et al.,

113   2023; Zhang et al., 2024). Such compound hazards are more destructive than the individual extremes

114   (Matthews et al., 2019). The SECC region has experienced a considerable rise in surface ozone

115   concentrations during the period from 2013 to 2019 (X. Meng et al., 2022). Although the individual

116   effects of heatwaves and TCs on ozone have been emphasized, the effects of the compound extremes

117   of heat waves and TCs on ozone pollution have received limited attention.

118   In this study, we aim to investigate the impacts of the compound hazards of TCs and extreme

119   hot days (TC-HDs) on ozone pollution in SECC (105-125° E,10-35° N) based on the long-term

120   (2014-2019) observational records of air temperatures and TCs, reanalysis datasets of ground-level

121   ozone concentrations and meteorological parameters, and the GEOS-Chem model simulations. The

122   mechanisms contributing to these impacts are also analyzed. The study is organized as follows:

123   Section 2 presents the methods and data utilized, and Section 3 describes the spatial and temporal

124   variations of TC-HDs observed in SECC during 2014-2019. Section 4 describes the impacts of TC-

125   HDs on ozone concentration in SECC, with a focus on YRD and PRD regions. In Section 5, we

126   investigate the possible mechanisms for the anomalous ozone concentrations in SECC during TC-

127   HDs as well as the differences between YRD and PRD by investigating the meteorological

128   conditions and key chemical and physical process analysis with the GEOS-Chem model. Finally,

129   Section 6 provides a summary and discussion.

130   **2. Data and methods**

131   **2.1 Observational datasets**

132   In this work, we focus on the ozone pollution over SECC where is vulnerable to both severe

133   hot extremes and ozone pollution (Ma et al., 2019; P. Wang et al., 2022). A topographic map of the

134   SECC including the YRD and PRD regions is shown in Figure 1. The daily maximum air

135   temperatures (Tmax) from observational sites in the domain for the period 2014-2019 are provided

136   by the China Meteorological Administration (CMA). The best track dataset of TCs is also released

137   by CMA (accessible at https:// tcdata.typhoon.org.cn/zjljsjj_sm.html). This dataset includes the time,

138   location, and intensity of TCs, which records all TCs that have passed through the western North

139   Pacific (WNP) since 1949 (Lu et al., 2021; Ying et al., 2014).

140   **2.2 Reanalysis datasets**

141   The ground-level ozone concentrations for the period 2014-2019 are obtained from the high-

142   resolution and high-quality ground-level MDA8 ozone data (unit: $\mu g/m^3$) for China (ChinaHighO$_3$)

143   at a resolution of $0.1° \times 0.1°$, which is one of the series of the high-resolution and high-quality

144   ground-level air pollutants in China (Wei et al., 2022). The ChinaHighO$_3$ dataset provides reliable

145   estimates of MDA8 ozone, demonstrated by an average out-of-sample (out-of-station) coefficient

146   of determination of 0.87 (0.80) and a root-mean-square error of 17.10 (21.10) μg/m³ across China

147   (Wei et al., 2022).

148   Meteorological parameters including 2-meter air temperature (T2m), relative humidity (RH),

149   surface solar radiation downwards (SSRD), geopotential height (HGT), eastward wind (uwnd),

150   northward wind (vwnd), mean sea level pressure (MSLP), total cloud cover (TCC), vertical integral

151   of eastward water vapour flux, vertical integral of northward water vapour flux and vertically

152   integrated moisture divergence are from the fifth generation of the European Centre for Medium-

153   Range Weather Forecasts (ECMWF) reanalysis data (ERA5), the latest global atmospheric

154   reanalysis of ECMWF (Hersbach et al., 2020). The temporal resolution for T2m, SSRD, and TCC

155   is 6 hours, while that for other meteorological parameters is 3 hours, which are all utilized to

156   generate daily mean values.

157   **2.3 Identifications of extreme events**

158   Severe ozone pollution episodes generally occur in SECC during summertime, coinciding with

159   frequent heatwaves and TCs (Ji et al., et al., 2024; Shu et al., 2016). In this work, we focus on the

160   impacts of extreme high temperatures and TCs on surface ozone during summer only (June, July,

161   and August) in SECC, as outlined in Figure 1. P. Wang et al. (2022) pointed out that most TC tracks

162   over the western North Pacific passed through the SECC region during their lifetimes in the past

163   several decades. The hot days (HDs) are defined as dates when the number of high-temperature sites

164   (Tmax≥35℃) exceeds more than 40% of the total number of observation stations within the SECC.

165   We use the proportion of high-temperature sites exceeding 40% as a measure of HDs to ensure

166   adequate samples and extremely hot conditions over SECC during HDs. Note that the anomalies of

167   surface ozone concentrations exhibit consistent spatial patterns during HDs identified by with a

168   lower (30%) or higher (50%) criterion for the percentage of high-temperature sites (figures not

169   shown). In this work, we classify all HDs into two categories: tropical cyclone-hot days (TC-HDs)

170   and alone hot days (AHDs). TC-HDs are identified when hot days occur over the land regions within

171   SECC, concurrent with the passages of tropical cyclones through the area; and AHDs indicate hot

172   days that occur independently.

173   In this work, the least squares method is applied to fit the linear trend and the Student' s t-test

174   is used to test the significance of the trend ($\alpha = 0.05$). A p-value < 0.05 indicates the statistically

175   significant trend (as shown in Figure 2). The Student's t-test is also used to evaluate the significance

176   of the differences in ozone concentrations and meteorological variables between HD/TC-HDs and

177   the long-term climatology.

178   **2.4 GEOS-Chem model**

179   In this study, surface ozone concentrations during 2014-2019 are simulated by using the 3-D

180   global chemical transport model (GEOS-Chem, version 13.4.1) with a horizontal resolution of 2°

181   latitude $\times$ 2.5° longitude and 47 vertical layers from the surface to 0.01 hPa. The GEOS-Chem has

182   the fully coupled O_3–NO_x–hydrocarbon–aerosol chemical mechanisms (Pye et al., 2009; Sherwen

183   et al., 2016) used to simulate concentrations of gas-phase pollutants (such as ozone) and aerosols.

184   It is driven by assimilated meteorological data of version 2 of Modern-Era Retrospective analysis

185   for Research and Applications (MERRA2; Gelaro et al., 2017)

186   The anthropogenic emissions of ozone precursor gases, including CO, NOx, and non-methane

187 volatile organic compounds (NMVOCs) are provided by the Community Emissions Data System

188 (CEDS) (Hoesly et al., 2018). Methane (CH_4) concentrations are provided by the Global Monitoring

189 Division (GMD) of the National Oceanic and Atmospheric Administration (NOAA). Biomass

190 burning emissions are obtained from the Global Fire Emissions Database version 4 (GFEDv4) (Van

191 Der Werf et al., 2017). The biogenic emissions are estimated with the Model of Emissions of Gases

192 and Aerosols from Nature (MEGAN) version 2.1(Guenther et al., 2012). Our previous studies show

193 that GEOS-Chem model excels in accurately reproducing observed ozone concentrations and spatial

194 distributions in China (Yang et al., 2022, 2014).

195 Meteorological conditions can modulate surface ozone concentrations through affecting the

196 physical and chemical processes including chemical production, horizontal advection, vertical

197 advection, dry deposition and diffusion (Gong and Liao, 2019). In this work, we quantify the

198 contributions of individual processes to ozone changes using the model outputs of GEOS-Chem

199 (Gong and Liao, 2019; Ni et al., 2024; Shu et al., 2016). In the GEOS-Chem model, the change in

200 ozone over time step are caused by chemical production, horizontal advection, vertical advection,

201 dry deposition and diffusion, which can be used for separating out and quantifying the contributions

202 of individual physical and chemical processes to the changes in the simulated ozone concentrations

203 (Gong and Liao, 2019; Ni et al., 2024; Shu et al., 2016).

204 **3. Spatial and temporal variations of compound TC-HDs**

205 There are 63 days of TC-HDs over SECC during the summers of 2014-2019, accounting for

206 around 70% of the total HDs (91 days), with 28 hot days (30%) occurring alone (AHDs) in the past

207 6 years. The monthly variations of HDs, TCs, and TC-HDs over SECC from 2014 to 2019 are

208　displayed in Figure 2. All the weather extremes show notable intraseasonal variations with relatively

209　higher occurrences in July and August but lower occurrences in June each year. Besides, both the

210　occurrences of HDs and TCs demonstrate significant upward trends at the 90% confidence level,

211　with a rate of 0.31 days per month and 0.33 days per month, respectively. TC-HDs also show an

212　increasing trend with a rate of increase of 0.2 days/month, consistent with the variations of HDs and

213　TCs in the past six years. Hence, it is essential to examine the effects of rising TC-HDs on ozone

214　pollution in the SECC region.

215　　　Figure 3 demonstrates the spatial features of TC-HDs during 2014-2019. China Meteorological

216　Administration classifies tropical cyclones into 6 classes based on their intensity, namely Tropical

217　Depression (TD, 10.8-17.1 m/s), Tropical Storm (TS, 17.2-24.4 m/s), Strong Tropical Storm (STS,

218　24.5-32.6 m/s), Typhoon (TY, 32.7-41.4 m/s), Strong Typhoon (STY, 41.5-50.9 m/s) and Super

219　Typhoon (SSTY, $\geq$51.0 m/s). TCs are generally stronger before their landfalls, which can reach STY

220　and even SSTY (Fig. 3a and 3b), consistent with previous findings (Han et al., 2022; Tuleya et al.,

221　1984).　TCs that affect the SECC primarily originate east of 135° E and move westward to the

222　eastern coastal regions. Around 90% of TCs associated with TC-HDs make landfalls while the

223　others weaken and dissipate over the ocean. Moreover, the air temperatures over land regions of

224　SECC during the TC-HDs are generally high, where the average Tmax of most sites are beyond 35℃

225　and reach up to 38℃ (Fig. 3a). Compared with the summer climatology from 2014 to 2019, the

226　average Tmax during TC-HDs increased approximately 4℃ over most land regions of SECC (Fig.

227　3b).

228　　　The temporal variations of the proportion of high-temperature sites (Tmax$\geq$ 35℃) and the

229　temperature anomalies relative to the summertime climatology averaged for the SECC land regions

230　along with the movements of TCs are given in Figs. 3c and 3d. Specifically, in Figures 3c&3d, the

231　colored dots along the movements of TC tracks represent the proportion of high-temperature sites

232　and the average temperature anomalies relative to the summertime climatology in SECC,

233　respectively. The two variables demonstrate similar patterns of variation. As TCs approach land

234　regions, both the high-temperature sites and temperature anomalies are increasing gradually, with a

235　particularly pronounced temperature increase associated with TCs moving towards the PRD regions.

236　In contrast, there is typically a decline in both the average air temperatures and the proportion of

237　high-temperature sites following the landfalls of TCs, which could be related to the strong wind and

238　rainfall associated with the TCs (Gori et al., 2022; Zhang et al. 2024).

239　4. Influences of TC-HDs on surface ozone concentrations in SECC

240　　Extreme high temperatures and the accompanied meteorology such as high-pressure systems

241　and strong radiation can affect local ozone pollution by enhancing chemical production and/or

242　accumulation (Gong and Liao, 2019; P. Wang et al., 2022; X. Wang et al., 2009). It is also well

243　demonstrated that extreme high temperatures and TCs can affect ozone pollution in coastal regions

244　of China (Ding et al., 2023; Huang et al., 2011; N. Wang et al., 2022). In this work, we further focus

245　on the impacts of TC-HDs on surface ozone concentrations over land regions of SECC. Figure 4

246　presents the spatial distributions of ozone concentration anomalies during TC-HDs and AHDs

247　relative to the summertime climatology from 2014-2019, as well as the differences between the two.

248　Notable increases in surface ozone concentrations are observed over most land regions of SECC

249　during the AHDs period, with anomalous MDA8 ozone reaching 40 $\mu g/m^3$ and 20 $\mu g/m^3$ over the

250   YRD (118-122° E, 30-33° N) and PRD (110-115.5° E, 21.5-24° N) regions, respectively (Fig. 4a),

251   consistent with previous finding that hot extremes can worsen ozone pollution (P. Wang et al., 2022).

252   During the compound TC-HDs, most land regions except Hainan Island and the northern part to 33°

253   N of SECC experience a significant enhancement in surface ozone concentrations, with MDA8

254   ozone anomalies above 20 $\mu g/m^3$ overall (Fig. 4b). Compared to AHDs, ozone concentrations in the

255   easternmost coastal regions of China including YRD (outlined in Fig. 4c) are suppressed while

256   ozone concentrations over the southernmost coastal regions of China including PRD (outlined in

257   Fig. 4c) are promoted during the compound TC-HDs. Comparing to TCs occurring alone, surface

258   ozone concentrations over most land regions of SECC increase during TC-HDs (Fig. S1), which

259   should be attributed to the increases in air temperatures. In this work, we investigate the enhanced

260   surface ozone concentration of PRD and the contrasting depression over YRD during the compound

261   TC-HDs.

262   The temporal variations of anomalous MDA8 ozone in YRD and PRD regions relative to the

263   summertime climatology with TC tracks during TC-HDs are shown in Figure 5. In Figures 5a&5b,

264   the colored dots along the TCs track represents the anomalies of regional mean MDA8 ozone

265   concentrations for YRD and PRD at that time compared with the summertime climatology for 2014-

266   2019. Surface ozone concentrations over YRD are abnormally higher when TCs are positioned a

267   long distance from land regions, whereas ozone concentrations fall dramatically when TCs approach

268   and make landfall over land regions. And it should be noted that the surface ozone concentrations

269   are elevated by the TCs moving westward YRD while most of the other TCs cause a decline in

270   ozone concentrations with their approach to land regions, consistent with previous work (Shu et al.,

271   2016). Zhan et al. (2020) revealed that O_3 pollution episodes in YRD mainly occurred near the 24-

272   hour warning line before a TC landed on the coastline. The region was impacted by an inland wind

273   carrying substantial precursor substances from polluted areas, while approaching TCs led to

274   increased precipitation and strong winds resulting in decreased ozone concentrations. For PRD,

275   surface ozone concentrations increase noticeably when TCs approaching land regions. Particularly,

276   TCs heading northeast to YRD favor the increases in ozone concentrations in the PRD whereas the

277   other TC tracks tend to cause a reduction in surface ozone concentrations following landfalls (Fig.

278   5b).

279   **5. Possible mechanisms underlying the impacts of TC-HDs on surface ozone**

280   **5.1 The dominant synoptic circulations**

281   The synoptic meteorological conditions during AHDs and TC-HDs are analyzed to disentangle

282   the different responses of surface ozone to hot extremes superimposed by TCs. Specifically, we

283   examine the composites of daily mean air temperature at 2m (T2m), relative humidity (RH), surface

284   solar radiation downwards (SSRD), mean sea level surface (MSLP), geopotential height at 500 hPa

285   (500hPa HGT) and 10-meter wind speeds, and total cloud cover (TCC) anomalies relative to

286   summertime climatology from 2014 to 2019 during AHDs (Fig. 6) and TC-HDs (Fig. 7), as well as

287   the differences between the two periods (Fig. 8). During the AHDs period, the land regions of SECC

288   are covered by increased T2m, decreased RH, reduced TCC, and enhanced SSRD (Figs. 6a-d),

289   which are favorable for the chemical formation of ozone therein (Yin et al., 2019), supporting the

290   elevated surface ozone during AHDs as shown in Figure 4a. In the mid-upper troposphere, a band

291   of positive HGT at 500hPa (H500) anomalies predominates over most land regions of China,

14

292 extending northeastward to Korea (Fig. 6e). This pattern features westerly wind anomalies in the

293 northern flank and easterly wind anomalies in the southern flank, indicating a westward extension

294 and strengthening of the western North Pacific subtropical high (WNPSH). These conditions favor

295 the occurrences of hot extremes over southern China, as discussed by Luo & Lau (2017) and P.

296 Wang et al. (2018). Besides, it's noticed that negative H500 anomalies and cyclonic circulation

297 appear over the east of 125°E which are also seen at the surface (Fig. 6f) with anomalous

298 southwesterly prevails over SECC land regions at the surface (Fig. 6f). Such a low-pressure system

299 characterizes TC track which finally recurve northeastward (Fig. S2).

300   During TC-HDs, most land regions of SECC are covered by increased T2m, decreased RH,

301 reduced TCC, and enhanced SSRD (Figs. 7a-d), favoring the enhanced chemical formation of ozone

302 therein, supporting the elevated surface ozone during TC-HDs as shown in Figure 4b. In the mid-

303 upper troposphere, positive H500 anomalies cover nearly the whole land region of China with

304 maximum dominating Korea, accompanied by anomalous anticyclonic circulation. Such changes

305 characterize the strengthening and westward extension of WPSH (Fig. 7e), favoring more hot

306 extremes. A dipole pattern of MSLP anomalies can be observed at the surface, with an abnormal

307 low-pressure center over the South China Sea and another to its east (Fig. 7f). Besides, the land

308 regions are influenced by weak winds at the surface (Fig. 7f). Particularly, for the decrease MDA8

309 ozone, we can see that during TC-HDs, Hainan island is covered by decreased T2m, increased RH,

310 reduced SSRD, and increased TCC (Figs. 7a-d), along with negative H500 and MSLP anomalies

311 (Figs. 7e&f). Such meteorological conditions in Hainan islands may suppress the chemical

312 production of ozone and the oceanic winds may clean the air (Fig. 7e). On the other hand, for the

15

313 north part of SECC, the circulation anomalies favor strengthened southeastern moisture flow and

314 enhance the convergence of water vapor flux there (Fig. S3), which can lead to increased relative

315 humidity (Fig.7b). The local higher temperature (Fig. 7a) and humid conditions may favor

316 convection activities (P. Wang et al., 2019b), characterized increased cloud cover (Fig. 7d) and

317 decreased surface solar radiation (Fig. 7c). These meteorological conditions can inhibit the local

318 ozone production and cause a lower ozone concentration in north part of the SECC during TC-HDs.

319   Figure 8 demonstrates the differences in meteorological variables between the periods of TC-

320 HDs and AHDs. Compared to AHDs, the YRD experiences an increase in T2m of approximately

321 1℃, while the PRD experiences a decrease in T2m of around 0.5℃ during TC-HDs. In the

322 meanwhile, RH and TCC values are increased (decreased) in PRD (YRD) while SSRD values are

323 decreased (increased) in PRD (YRD) (Figs. 8a-d). The large-scale circulations in the middle-upper

324 troposphere show positive H500 anomalies over the north and northeast parts of China including

325 YRD while southern China including PRD is dominated by negative H500 anomalies, supporting

326 the increased T2m (decreased) over YRD (PRD). Moreover, a cyclonic circulation controls southern

327 China with YRD influenced by strong southeasterly winds while PRD is influenced by inland

328 northeasterly winds (Fig. 8e). The changes in MSLP show a similar pattern to H500 anomalies with

329 positive anomalies over YRD but negative anomalies over PRD, and an anomalous low-pressure

330 system is observed over South China Sea, accompanied by strong cyclonic circulation at the surface.

331 It should be noted that the YRD is influenced by strong easterly winds from the ocean which may

332 alleviate ozone pollution as shown in Figure 4c. In contrast, PRD is influenced by strong

333 northeasterly winds from inland which is opposite to the climatological southwesterlies of the

334   summer monsoon circulation, which may favor the accumulation of ozone pollution therein, as

335   shown in Fig. 4c

336   It should be noted that the mereological conditions in YRD favor the chemical production of

337   ozone yet reduced ozone concentrations are observed in YRD during TC-HDs relative to AHDs.

338   The key physiochemical processes associated with the alleviated ozone pollution over YRD but

339   worsened ozone pollution over RPD during TC-HDs relative to AHDs are explored with GEOS-

340   Chem model simulations in the following part.

341   **5.2 Process analysis with GEOS-Chem model simulations**

342   In this section, process analysis is conducted in the GEOS-Chem model to quantify the

343   contributions of each process, including net chemical production, horizontal advection, vertical

344   advection, and mixing (diffusion and dry deposition) to the anomalous surface ozone concentrations

345   over PRD and YRD during TC-HDs, respectively. The observed and simulated anomalous surface

346   MDA8 ozone during TC-HDs relative to the summer climatology mean and AHDs are given in

347   Figure S4 and the regional averages of surface MDA8 ozone concentrations over YRD and PRD

348   are summarized in Table 1. GEOS-Chem simulation can reasonably capture the spatial pattern of

349   anomalous surface MDA8 ozone concentrations during TC-HDs relative to the summer climatology

350   mean (Figs. S4a and b), and relative to AHDs (Figs. S4c and d). Particularly, compared to AHDs,

351   the simulated surface MDA8 ozone concentrations are inhibited over YRD but enhanced over PRD

352   during TC-HDs. As listed in Table 1, compared to AHDs, during TC-HDs, the observed (simulated)

353   average surface MDA8 ozone concentrations in the YRD decreased by 13.21 μg/m³ (21.94 μg/m³),

354   whereas it increased by 6.8 μg/m³ (7 μg/m³) in the PRD. This suggests that the model simulation

17

355 can reasonably capture the opposite changes in surface MDA8 ozone concentrations over the YRD

356 and PRD during extreme HDs superimposed by TCs.

357   Figure 9 illustrates the vertical profiles of simulated daily mean ozone concentrations for YRD

358 and PRD from surface to 500 hPa for the summer climatology, TC-HDs and AHDs during 2014-

359 2019, respectively. For YRD, surface ozone concentrations are apparently higher during AHDs than

360 those during TC-HDs and summertime climatology from surface up to the 500 hPa level (Fig. 9a).

361 This indicates that the enhancements in ozone concentrations during AHDs occur not only at the

362 surface but also to the middle of the troposphere. In addition, compared with the summertime

363 climatology, ozone concentrations in YRD during TC-HDs are slightly enhanced from surface to

364 850 hPa as well as between 600 hPa and 500 hPa while suppressed between 850hPa and 600 hPa.

365 For the PRD, ozone concentrations during TC-HDs are higher than the summertime mean and AHDs

366 from the surface up to 500 hPa (Fig. 9b). The ozone concentrations during AHDs are comparable to

367 (slightly stronger than) the summertime mean below (above) 850 hPa (Fig. 9b) based on the GEOS-

368 Chem model simulation.

369   We further analyze the main physiochemical processes affecting ozone concentration,

370 including net chemical production, vertical advection, horizontal advection and mixing (the sum of

371 dry deposition and diffusion). Figures 10 and 11 show the vertical profiles of the anomaly of each

372 process during TC-HDs and AHDs, relative to the summertime climatology over the YRD and PRD,

373 as well as the differences between TC-HDs and AHDs. During AHDs, the increase in ozone

374 concentrations in the YRD from the surface to 900 hPa is primarily contributed by chemical

375 production, while transport processes tend to decrease ozone concentration. Between 900 hPa and

18

376   700 hPa, the mixing process contributes to the increases in ozone concentrations while the transport

377   processes and chemical productions tend to decrease ozone concentrations. Between 700 hPa and

378   500 hPa, horizontal transport hampers ozone increase, while chemical production and vertical

379   transport contribute to ozone enhancement (Fig. 10a). During TC-HDs, the horizontal transport

380   exhibits a suppressive effect on ozone concentrations in the YRD from the surface up to 500 hPa

381   whereas the chemical production contributes to increases in ozone concentration. And two processes

382   overtake the effects of vertical transport and mixing (Fig. 10b). In comparison with AHDs, during

383   TC-HDs, ozone concentration increases due to chemical production exceed decreases caused by

384   horizontal transport between the surface and 850 hPa. However, between 850 hPa and 700 hPa, the

385   decrease in ozone concentration due to horizontal transport outweighs the increase from chemical

386   production. Overall, compared to AHDs, the chemical production contributes to increased ozone

387   concentrations in the YRD from the surface up to 500 hPa during TC-HDs, whereas the horizontal

388   transport tends to lower ozone concentrations. The relatively small differences in physicochemical

389   processes between AHDs and TC-HDs around 700 hPa in the vertical profile are due to the minor

390   effects of these processes during both AHDs and TC-HDs (not shown). As listed in Table 2,

391   compared to AHDs, ozone chemical production plays a predominant role in enhancing ozone

392   pollution during TC-HDs in the YRD (1.24 Gg O_3/day), whereas horizontal transport significantly

393   depresses ozone concentration (-1.15 Gg O_3/day). As stressed above, the strong and oceanic winds

394   along YRD can help alleviate ozone pollution. The vertical transport and mixing processes play a

395   less important role in affecting ozone concentrations in YRD during TC-HDs.

396   For PRD, the horizontal transport primarily contributes to decreased ozone concentrations in

the PRD between the surface and 500 hPa during AHDs. The chemical production, vertical transport

and mixing processes exhibit promoting effects on ozone concentrations from surface to 700 hPa

(Fig. 11a). During TC-HDs, horizontal transport predominantly contributes to increased ozone

concentrations over PRD from surface to 900 hPa and between 850 hPa and 500 hPa and the

chemical production increases ozone concentrations between 950 hPa and 800 hPa. In contrast, the

mixing process and vertical transport play a dominant role in reducing ozone concentrations

between the surface to 900 hPa and between 900 hPa to 500 hPa respectively (Fig. 11b). Compared

to AHDs, during TC-HDs, transport processes predominantly contribute to the increases in ozone

concentrations in the PRD from the surface up to 500 hPa. Additionally, between 900 hPa and 800

hPa, chemical production plays a positive role in enhancing ozone concentrations. As listed in Table

3, during TC-HDs compared to AHDs, the horizontal transport process in the PRD exhibits a

significantly stronger enhancing effect on ozone concentrations from surface to 500 hPa (1.81 Gg

O_3/day) compared to the other three processes. Note that the summer climatology of ozone

concentrations in YRD is significantly higher than that in PRD (Fig. S5) and the cross-section of

wind anomalies demonstrates that strong winds from YRD to PRD exist during TC-HDs (Fig. S6),

implying strong ozone mass transport from YRD to PRD. Thus, the cross-region transport may play

a significant role in worsening ozone pollution over RPD during TC-HDs relative to AHDs.

In summary, favorable synoptic patterns during extreme hot days promote the chemical

production of ozone, and thus exacerbate ozone pollution over both YRD and PRD. Compared to

AHDs, the anomalously meteorological conditions during TC-HDs, enhance the chemical

production of ozone in the YRD while the horizontal transport process mitigates ozone pollution

20

418   therein but worsens ozone pollution in PRD though cross-regional transport, finally resulting in an

419   increase in ozone in PRD but a decrease in YRD.

420   **6. Conclusion and discussions**

421   China has implemented a series of emission reduction strategies to alleviate air pollution, and

422    $PM_{2.5}$ concentrations have decreased significantly while ozone pollution remains a major concern.

423   Ozone pollution is sensitive to meteorological conditions, especially the extreme weathers that

424   frequently strike China under global warming. Eastern China is economically developed and

425   densely populated, with serious ozone pollution. It is also vulnerable to both extreme hot weathers

426   and TCs during the summer, which can substantially affect surface ozone concentrations (Lin et al.,

427   2019; T. Wang et al., 2017). High ozone levels are generally linked to high air temperatures, which

428   increase BVOC emissions and enhance ozone formation (e.g., Lu et al., 2019; P. Wang et al., 2022).

429   TC activities can modify surface ozone concentrations by affecting the transport and accumulation

430   processes, exacerbating pollution in the YRD and PRD (e.g., Shu et al., 2016; Zhan et al., 2020).

431   The SECC region experiences both frequent TCs and heatwave events under global warming (W.

432   Wang et al., 2016; Xiao et al., 2011) which has proven to have an intrinsic concurrent relationship

433   (Matthews et al., 2019; P. Wang et al., 2023). However, the impacts of the compound extremes of

434   hot extremes and TCs on ozone pollution over SECC have received limited attention.

435   In this work, we systematically investigate the impacts of extreme hot weathers on surface

436   ozone for the summers of 2014-2019 over SECC coupled with (TC-HDs) and without TCs (AHDs).

437   The associated synoptic conditions and physicochemical processes are assessed combined

438   reanalysis dataset with the GEOS-Chem model simulations.

439   Results show that the surface ozone concentrations over most land regions within SECC are

440 elevated during both TC-HDs and AHDs relative to the climatological mean, however, there are

441 considerable differences between the changes in ozone concentrations during TC-HDs and AHDs.

442 Relative to AHDs, the surface ozone concentrations are noticeably decreased in the YRD region but

443 increased in the PRD region during TC-HDs periods. The meteorological conditions suggest that

444 though YRD is influenced by higher temperature, lower humidity, and stronger radiation during TC-

445 HDs than AHDs, it is influenced by strong and sea breezes, which aid in ozone elimination. In

446 contrast, the PRD is influenced by the strong northeasterly winds, opposite to the climatology, and

447 may transport ozone pollution from polluted regions. Such a hypothesis is validated with the GEOS-

448 Chem simulation. Compared with AHDs, among all the physicochemical processes, horizontal

449 transport plays a crucial role in increasing (reducing) ozone levels over PRD (YRD). Compared to

450 AHDs, the horizontal transport contributes to -1.15 Gg O_3/day and 1.8 Gg O_3/day to the net

451 changes in tropospheric ozone mass from surface to 500 hPa in YRD and PRD during TC-HDs. The

452 findings will provide significant implications for the control measures of ozone pollution in PRD

453 and YRD during hot extremes, to consider the significant impacts of TC activities.

454   Note that throughout the lifetime of tropical cyclones, their positions exert varying influences

455 on air temperatures and surface ozone concentrations over the land regions. Extremely high

456 temperatures are typically observed before TCs make landfalls, driven by descending motions and

457 intensified solar radiation (Wang et al., 2023). However, the high temperatures rapidly decline once

458 TCs make landfalls, primarily due to the accompanying strong winds and precipitation (Gori et al.,

459 2022; Zhang et al., 2024). Similarly, surface ozone concentrations over the YRD and PRD

regions tend to be elevated when TCs are at a distance from the land regions but they fall dramatically when TCs make landfalls (Fig. 5), consistent with previous findings (e.g., Zhan et al., 2020).

Extreme hot weathers are projected to be more frequent and intensified in the future under the continued global warming (P. Wang et al., 2019a). Moreover, it is projected that TCs and heatwave compound events are projected to significantly increase in their intensity and frequency over the Northwest Pacific, causing potentially enlarged population exposures for the southeastern coast of China (Wu et al. 2022). Therefore, the potential impacts of extreme hot weather and the TC-HDs on surface ozone over China warrants future efforts. BVOCs are important precursors of ozone, and their emissions are greatly influenced by weather conditions. As revealed by N. Wang et al. (2022), the TCs over Northwest Pacific could intensify the chemical interactions between anthropogenic and biogenic emissions, resulting in extreme ozone pollution over YRD and PRD regions. The responses of biogenic emissions during hot extremes accompanied by TCs deserve further investigation.

Data availability

The ground-level ozone concentrations are obtained from the high-resolution and high-quality ground-level daily maximum 8-hour average ozone (MDA8 O_3) data for China (ChinaHighO$_3$, https://doi.org/10.5281/zenodo.4400043). Daily maximum air temperature is provided by the National Meteorological Information Center of the China Meteorological Administration (CMA, http://data.cma.cn/en/). The best track dataset of tropical cyclones is also released by CMA (https://

481 tcdata.typhoon.org.cn/zjljsjj_sm.html). Meteorological conditions data are derived from the fifth

482 generation of ECMWF reanalysis data (ERA5, https://cds.climate.copernicus.eu/). The GEOS-

483 Chem model is available at http://acmg.seas.harvard.edu/geos/.

484 **Author contributions**

485 C. Qi performed the analyses and wrote the initial draft. P. Wang and Y. Yang conceived and

486 supervised the study. H. Li performed the GEOS-Chem simulations. P. Wang reviewed and edited

487 the initial draft. All the authors discussed the results and contributed to the final manuscript.

488 **Competing interests**

489 The authors declare that they have no competing interest.

490 **Acknowledgements**

496

References

Ainsworth, E.A., Yendrek, C.R., Sitch, S., Collins, W.J., Emberson, L.D.: The Effects of Tropospheric Ozone on Net Primary Productivity and Implications for Climate Change, Annu. Rev. Plant Biol., 63, 637–661, https://doi.org/10.1146/annurev-arplant-042110-103829, 2012.

Ashmore, M.R.: Assessing the future global impacts of ozone on vegetation, Plant Cell Environ., 28, 949–964, https://doi.org/10.1111/j.1365-3040.2005.01341.x, 2005.

Banta, R.M., Senff, C.J., Alvarez, R.J., Langford, A.O., Parrish, D.D., Trainer, M.K., Darby, L.S., Michael Hardesty, R., Lambeth, B., Andrew Neuman, J.: Dependence of daily peak O_3 concentrations near Houston, Texas on environmental factors: Wind speed, temperature, and boundary-layer depth, Atmos. Environ., 45, 162–173, https://doi.org/10.1016/j.atmosenv.2010.09.030, 2011.

Chen, L., Liao, H., Zhu, J., Li, K., Bai, Y., Yue, X., Yang, Y., Hu, J., Zhang, M.: Increases in ozone-related mortality in China over 2013–2030 attributed to historical ozone deterioration and future population aging, Sci. Total Environ., 858, 159972, https://doi.org/10.1016/j.scitotenv.2022.159972, 2023.

Dai, H., Huang, G., Wang, J., Zeng, H.: VAR-tree model based spatio-temporal characterization and prediction of O_3 concentration in China, Ecotoxicol. Environ. Saf., 257, 114960, https://doi.org/10.1016/j.ecoenv.2023.114960, 2023.

Ding, H., Kong, L., You, Y., Mao, J., Chen, W., Chen, D., ... & Wang, X.: Effects of tropical cyclones with different tracks on ozone pollution over the Pearl River Delta region, Atmos. Res., 286, 106680, https://doi.org/10.1016/j.atmosres.2023.106680, 2023

Feng, Z., Hu, E., Wang, X., Jiang, L., Liu, X.: Ground-level O_3 pollution and its impacts on food crops in China: A review, Environ. Pollut., 199, 42–48, https://doi.org/10.1016/j.envpol.2015.01.016, 2015.

Fu, Y., Liao, H.: Impacts of land use and land cover changes on biogenic emissions of volatile organic compounds in China from the late 1980s to the mid-2000s: implications for tropospheric ozone and secondary organic aerosol, Tellus B Chem. Phys. Meteorol., 66, 24987, https://doi.org/10.3402/tellusb.v66.24987, 2014.

Fu, Y., Liao, H., Yang, Y.: Interannual and Decadal Changes in Tropospheric Ozone in China and the Associated Chemistry-Climate Interactions: A Review, Adv. Atmospheric Sci., 36, 975–993, https://doi.org/10.1007/s00376-019-8216-9, 2019.

Gelaro, R., McCarty, W., Suárez, M. J., Todling, R., Molod, A., Takacs, L., Randles, C. A., Darmenov, A., Bosilovich, M. G., Reichle, R., Wargan, K., Coy, L., Cullather, R., Draper, C., Akella, S., Buchard, V., Conaty, A., Da Silva, A. M., Gu, W., … Zhao, B.: The Modern-Era Retrospective Analysis for Research and Applications, Version 2 (MERRA-2), J. Climate, 30, 5419–5454, https://doi.org/10.1175/JCLI-D-16-0758.1, 2017.

Gong, C., Liao, H.: A typical weather pattern for ozone pollution events in North China, Atmospheric Chem. Phys., 19, 13725–13740, https://doi.org/10.5194/acp-19-13725-2019, 2019.

Gori, A., Lin, N., Xi, D., & Emanuel, K.: Tropical cyclone climatology change greatly exacerbates US extreme rainfall–surge hazard, Nat. Clim. Chang., 12, 171–178, https://doi.org/10.1038/s41558-021-01272-7, 2022.

539   Gu, X., Wang, T., Li, C.: Elevated ozone decreases the multifunctionality of belowground

540   ecosystems, Glob. Change Biol., 29, 890–908, https://doi.org/10.1111/gcb.16507, 2023.

541   Guenther, A.B., Jiang, X., Heald, C.L., Sakulyanontvittaya, T., Duhl, T., Emmons, L.K., Wang, X.:

542   The Model of Emissions of Gases and Aerosols from Nature version 2.1 (MEGAN2.1): an

543   extended and updated framework for modeling biogenic emissions, Geosci. Model Dev., 5,

544   1471–1492, https://doi.org/10.5194/gmd-5-1471-2012, 2012.

545   Han, W., Wang, Y., & Liu, L.: The relationship between pre-landfall intensity change and post-

546   landfall weakening of tropical cyclones over China, Front. Earth Sci., 10, 1082181,

547   https://doi.org/10.3389/feart.2022.1082181, 2022.

548   H. Hersbach, B. Bell, P. Berrisford, S. Hirahara, A. Horányi, J. Muñoz-Sabater, J. Nicolas, C. Peubey,

549   R. Radu, D. Schepers, A. Simmons, C. Soci, S. Abdalla, X. Abellan, G. Balsamo, P. Bechtold,

550   G. Biavati, J. Bidlot, M. Bonavita, G. de Chiara, P. Dahlgren, D. Dee, M. Diamantakis, R.

551   Dragani, J. Flemming, R. Forbes, M. Fuentes, A. Geer, L. Haimberger, S. Healy, R. J. Hogan,

552   E. Hólm, M. Janisková, S. Keeley, P. Laloyaux, P. Lopez, C. Lupu, G. Radnoti, P. de Rosnay,

553   I. Rozum, F. Vamborg, S. Villaume, J. N. Thépaut,.: The ERA5 global reanalysis, Q. J. R.

554   Meteorol. Soc., 146(730), 1999-2049, https://doi.org/10.1002/qj.3803, 2020.

555   Hoesly, R.M., Smith, S.J., Feng, L., Klimont, Z., Janssens-Maenhout, G., Pitkanen, T., Seibert, J.J.,

556   Vu, L., Andres, R.J., Bolt, R.M., Bond, T.C., Dawidowski, L., Kholod, N., Kurokawa, J., Li,

557   M., Liu, L., Lu, Z., Moura, M.C.P., O'Rourke, P.R., Zhang, Q.: Historical (1750–2014)

558   anthropogenic emissions of reactive gases and aerosols from the Community Emissions Data

559   System (CEDS), Geosci. Model Dev., 11, 369–408, https://doi.org/10.5194/gmd-11-369-2018,

560 2018.

561 Huang, C., Chen, C. H., Li, L., Cheng, Z., Wang, H. L., Huang, H. Y., Streets, D. G., Wang, Y. J.,

562 Zhang, G. F., and Chen, Y. R.: Emission inventory of anthropogenic air pollutants and VOC

563 species in the Yangtze River Delta region, China, Atmos. Chem. Phys., 11, 4105–4120,

564 https://doi.org/10.5194/acp-11-4105-2011, 2011.

565 Huang, J., Pan, X., Guo, X., Li, G.: Health impact of China's Air Pollution Prevention and Control

566 Action Plan: an analysis of national air quality monitoring and mortality data, Lancet Planet.

567 Health, 2, e313–e323, https://doi.org/10.1016/S2542-5196(18)30141-4, 2018.

568 Jacob, D.J., Logan, J.A., Murti, P.P.: Effect of rising Asian emissions on surface ozone in the United

569 States, Geophys. Res. Lett., 26, 2175–2178, https://doi.org/10.1029/1999GL900450, 1999.

570 Jammalamadaka, S.R., Lund, U.J.: The effect of wind direction on ozone levels: a case study,

571 Environ. Ecol. Stat., 13, 287–298, https://doi.org/10.1007/s10651-004-0012-7, 2006.

572 Ji, X., Chen, G., Chen, J., Xu, L., Lin, Z., Zhang, K., Fan, X., Li, M., Zhang, F., Wang, H., Huang,

573 Z., & Hong, Y.: Meteorological impacts on the unexpected ozone pollution in coastal cities of

574 China during the unprecedented hot summer of 2022, Sci. Total Environ., 914, 170035,

575 https://doi.org/10.1016/j.scitotenv.2024.170035, 2024.

576 Jiang, Z., Li, J., Lu, X., Gong, C., Zhang, L., Liao, H.: Impact of western Pacific subtropical high

577 on ozone pollution over eastern China, Atmospheric Chem. Phys., 21, 2601–2613,

578 https://doi.org/10.5194/acp-21-2601-2021, 2021.

579 Kavassalis, S.C., Murphy, J.G.: Understanding ozone-meteorology correlations: A role for dry

580 deposition, Geophys. Res. Lett., 44, 2922–2931, https://doi.org/10.1002/2016GL071791, 2017.

581 Li, K., Jacob, D.J., Liao, H., Shen, L., Zhang, Q., Bates, K.H.: Anthropogenic drivers of 2013–2017

582   trends in summer surface ozone in China, Proc. Natl. Acad. Sci., 116, 422–427,

583   https://doi.org/10.1073/pnas.1812168116, 2019.

584 Li, M., Yu, S., Chen, X., Li, Z., Zhang, Y., Wang, L., Liu, W., Li, P., Lichtfouse, E., Rosenfeld, D.,

585   and Seinfeld, J. H.: Large scale control of surface ozone by relative humidity observed during

586   warm seasons in China, Environ. Chem. Lett., 19, 3981–3989, https://doi.org/10.1007/s10311-

587   021-01265-0, 2021.

588 Lin, X., Yuan, Z., Yang, L., Luo, H., Li, W.: Impact of Extreme Meteorological Events on Ozone in

589   the Pearl River Delta, China, Aerosol Air Qual. Res., 19, 1307–1324,

590   https://doi.org/10.4209/aaqr.2019.01.0027, 2019.

591 Liu, H., Liu, S., Xue, B., Lv, Z., Meng, Z., Yang, X., Xue, T., Yu, Q., He, K.: Ground-level ozone

592   pollution and its health impacts in China, Atmos. Environ., 173, 223–230,

593   https://doi.org/10.1016/j.atmosenv.2017.11.014, 2018.

594 Lu, X., Yu, H., Ying, M., Zhao, B., Zhang, S., Lin, L., Bai, L., Wan, R.: Western North Pacific

595   Tropical Cyclone Database Created by the China Meteorological Administration, Adv.

596   Atmospheric Sci., 38, 690–699, https://doi.org/10.1007/s00376-020-0211-7, 2021.

597 Lu, X., Zhang, L., Chen, Y., Zhou, M., Zheng, B., Li, K., Liu, Y., Lin, J., Fu, T.-M., Zhang, Q.:

598   Exploring 2016–2017 surface ozone pollution over China: source contributions and

599   meteorological influences, Atmospheric Chem. Phys., 19, 8339–8361,

600   https://doi.org/10.5194/acp-19-8339-2019, 2019.

601 Luo, M., & Lau, N.-C.: Heat Waves in Southern China: Synoptic Behavior, Long-Term Change, and

602   Urbanization Effects, J. Climate, 30(2), 703–720, https://doi.org/10.1175/JCLI-D-16-0269.1,

603   2017.

604   Ma, M., Gao, Y., Wang, Y., Zhang, S., Leung, L.R., Liu, C., Wang, S., Zhao, B., Chang, X., Su, H.,

605   Zhang, T., Sheng, L., Yao, X., Gao, H.: Substantial ozone enhancement over the North China

606   Plain from increased biogenic emissions due to heat waves and land cover in summer 2017,

607   Atmos Chem Phys., 19, 12195-12207, https://doi.org/10.5194/acp-19-12195-2019, 2019.

608   Matthews, T., Wilby, R.L., Murphy, C.: An emerging tropical cyclone–deadly heat compound hazard,

609   Nat. Clim. Change, 9, 602–606, https://doi.org/10.1038/s41558-019-0525-6, 2019.

610   Meng, K., Zhao, T., Xu, X., Hu, Y., Zhao, Yang, Zhang, L., Pang, Y., Ma, X., Bai, Y., Zhao, Yuguang,

611   Zhen, S.: Anomalous surface O_3 changes in North China Plain during the northwestward

612   movement of a landing typhoon, Sci. Total Environ., 820, 153196,

613   https://doi.org/10.1016/j.scitotenv.2022.153196, 2022.

614   Meng, X., Wang, W., Shi, S., Zhu, S., Wang, P., Chen, R., Xiao, Q., Xue, T., Geng, G., Zhang, Q.,

615   Kan, H., Zhang, H.: Evaluating the spatiotemporal ozone characteristics with high-resolution

616   predictions in mainland China, 2013–2019, Environ. Pollut., 299, 118865,

617   https://doi.org/10.1016/j.envpol.2022.118865, 2022.

618   Ni, Y., Yang, Y., Wang, H., Li, H., Li, M., Wang, P.: Contrasting changes in ozone during 2019–2021

619   between eastern China and the other regions of China, Sci. Total Environ., 908, 168272,

620   http://dx.doi.org/10.2139/ssrn.4563723, 2024.

621   Ouyang, S., Deng, T., Liu, R., Chen, J., He, G., Leung, J.C.H., Wang, N., Liu, S.C.: Impact of a

622   subtropical high and a typhoon on a severe ozone pollution episode in the Pearl River Delta,

China, Atmospheric Chem. Phys., 22(16), 10751-10767, https://doi.Org/10.5194/acp-22-10751-2022, 2022.

Pye, H.O.T., Liao, H., Wu, S., Mickley, L.J., Jacob, D.J., Henze, D.K., Seinfeld, J.H.: Effect of changes in climate and emissions on future sulfate-nitrate-ammonium aerosol levels in the United States, J. Geophys. Res. Atmospheres, 114, 2008JD010701, https://doi.org/10.1029/2008JD010701, 2009.

Qu, K., Wang, X., Yan, Y., Shen, J., Xiao, T., Dong, H., Zeng, L., Zhang, Y.: A comparative study to reveal the influence of typhoons on the transport, production and accumulation of O_3 in the Pearl River Delta, Atmospheric Chem. Phys., 21, 11593–11612, https://doi.org/10.5194/acp-21-11593-2021, 2021.

Sherwen, T., Schmidt, J.A., Evans, M.J., Carpenter, L.J., Großmann, K., Eastham, S.D., Jacob, D.J., Dix, B., Koenig, T.K., Sinreich, R., Ortega, I., Volkamer, R., Saiz-Lopez, A., Prados-Roman, C., Mahajan, A.S., Ordóñez, C.: Global impacts of tropospheric halogens (Cl, Br, I) on oxidants and composition in GEOS-Chem, Atmospheric Chem. Phys., 16, 12239–12271, https://doi.org/10.5194/acp-16-12239-2016, 2016.

Shu, L., Xie, M., Wang, T., Gao, D., Chen, P., Han, Y., Li, S., Zhuang, B., Li, M.: Integrated studies of a regional ozone pollution synthetically affected by subtropical high and typhoon system in the Yangtze River Delta region, China, Atmospheric Chem. Phys., 16, 15801–15819, https://doi.org/10.5194/acp-16-15801-2016, 2016.

Song, X., Hao, Y.: An assessment of O_3-related health risks and economic losses in typical regions of China, Front. Public Health, 11, 1194340, https://doi.org/10.3389/fpubh.2023.1194340,

644   2023.

645   Tuleya, R. E., Bender, M. A., and Kurihara, Y.: A Simulation Study of the Landfall of Tropical

646   Cyclones, Mon. Wea. Rev., 112, 124–136, https://doi.org/10.1175/1520-

647   0493(1984)112<0124:ASSOTL>2.0.CO;2, 1984.

648   Turner, M.C., Jerrett, M., Pope, C.A., Krewski, D., Gapstur, S.M., Diver, W.R., Beckerman, B.S.,

649   Marshall, J.D., Su, J., Crouse, D.L., Burnett, R.T.: Long-Term Ozone Exposure and Mortality

650   in a Large Prospective Study, Am. J. Respir. Crit. Care Med, 193, 1134–1142,

651   https://doi.org/10.1164/rccm.201508-1633OC, 2016.

652   Van Der Werf, G.R., Randerson, J.T., Giglio, L., Van Leeuwen, T.T., Chen, Y., Rogers, B.M., Mu,

653   M., Van Marle, M.J.E., Morton, D.C., Collatz, G.J., Yokelson, R.J., Kasibhatla, P.S.: Global

654   fire emissions estimates during 1997–2016, Earth Syst. Sci. Data, 9, 697–720,

655   https://doi.org/10.5194/essd-9-697-2017, 2017.

656   Wang, N., Huang, X., Xu, J., Wang, T., Tan, Z., Ding, A.: Typhoon-boosted biogenic emission

657   aggravates cross-regional ozone pollution in China, Sci. Adv., 8, eabl6166,

658   https://doi.org/10.1126/sciadv.abl6166, 2022.

659   Wang, P., Hui, P., Xue, D., & Tang, J.: Future projection of heat waves over China under global

660   warming within the CORDEX-EA-II project, Clim. Dynam., 53(1–2), 957–973,

661   https://doi.org/10.1007/s00382-019-04621-7, 2019a.

662   Wang, P., Leung, L. R., Lu, J., Song, F., & Tang, J.: Extreme wet-bulb temperatures in China: The

663   significant role of moisture, J. Geophys. Res.: Atmos., 124(22), 11944–11960,

664   https://doi.org/10.1029/2019JD031477, 2019b.

Wang, P., Tang, J., Wang, S., Dong, X., & Fang, J.: Regional heatwaves in china: a cluster analysis, Clim. Dynam., 50, 1901–1917, https://doi.org/10.1007/s00382-017-3728-4, 2018.

Wang, P., Yang, Y., Li, H., Chen, L., Dang, R., Xue, D., Li, B., Tang, J., Leung, L.R., Liao, H.: North China Plain as a hot spot of ozone pollution exacerbated by extreme high temperatures, Atmospheric Chem. Phys., 22, 4705–4719, https://doi.org/10.5194/acp-22-4705-2022, 2022.

Wang, P., Yang, Y., Xue, D., Qu, Y., Tang, J., Leung, L.R., Liao, H.: Increasing Compound Hazards of Tropical Cyclones and Heatwaves over Southeastern Coast of China under Climate Warming, J. Clim., 36, 2243–2257, https://doi.org/10.1175/JCLI-D-22-0279.1, 2023.

Wang, T., Xue, L., Brimblecombe, P., Lam, Y.F., Li, L., Zhang, L.: Ozone pollution in China: A review of concentrations, meteorological influences, chemical precursors, and effects, Sci. Total Environ., 575, 1582–1596, https://doi.org/10.1016/j.scitotenv.2016.10.081, 2017.

Wang, T., Zhong, Z., Sun, Y., Wang, J.: Impacts of tropical cyclones on the meridional movement of the western Pacific subtropical high, Atmospheric Sci. Lett., 20, e893, https://doi.org/10.1002/asl.893, 2019.

Wang, W., Zhou, W., Li, X., Wang, X., Wang, D.: Synoptic-scale characteristics and atmospheric controls of summer heat waves in China, Clim. Dynam., 46, 2923–2941, https://doi.org/10.1007/s00382-015-2741-8, 2016.

Wang, X., Chen, F., Wu, Z., Zhang, M., Tewari, M., Guenther, A., & Wiedinmyer, C.: Impacts of weather conditions modified by urban expansion on surface ozone: Comparison between the Pearl River Delta and Yangtze River Delta regions, Adv. Atmos. Sci., 26, 962–972, https://doi.org/10.1007/s00376-009-8001-2, 2009.

Wang, Z., Hu, B., Zhang, C., Atkinson, P.M., Wang, Z., Xu, K., Chang, J., Fang, X., Jiang, Y., Shi, Z.: How the Air Clean Plan and carbon mitigation measures co-benefited China in $PM_{2.5}$ reduction and health from 2014 to 2020, Environ. Int., 169, 107510 https://doi.org/10.1016/j.envint.2022.107510, 2022.

Wei, J., Li, Z., Li, K., Dickerson, R.R., Pinker, R.T., Wang, J., Liu, X., Sun, L., Xue, W., Cribb, M.: Full-coverage mapping and spatiotemporal variations of ground-level ozone (O_3) pollution from 2013 to 2020 across China, Remote Sens. Environ., 270, 112775, https://doi.org/10.1016/j.rse.2021.112775, 2022.

Wei, X., Lam, K. S., Cao, C., Li, H., & He, J.: Dynamics of the Typhoon Haitang Related High Ozone Episode over Hong Kong, Adv. Atmospheric Sci., 6089154, https://doi.org/10.1155/2016/6089154, 2016.

Wu, J., Chen, Y., Liao, Z., Gao, X., Zhai, P., & Hu, Y.: Increasing risk from landfalling tropical cyclone-heatwave compound events to coastal and inland China, Environ. Res. Lett., 17(10), 105007, https://doi.org/10.1088/1748-9326/ac9747, 2022.

Xiao, Y.F., Duan, Z.D., Xiao, Y.Q., Ou, J.P., Chang, L., Li, Q.S.: Typhoon wind hazard analysis for southeast China coastal regions, Struct. Saf., 33, 286–295, https://doi.org/10.1016/j.strusafe.2011.04.003, 2011.

Yang, Y., Li, M., Wang, H., Li, H., Wang, P., Li, K., Gao, M., Liao, H.: ENSO modulation of summertime tropospheric ozone over China, Environ. Res. Lett., 17, 034020, https://doi.org/10.1088/1748-9326/ac54cd, 2022.

Yang, Y., Liao, H., Li, J.: Impacts of the East Asian summer monsoon on interannual variations of

summertime surface-layer ozone concentrations over China, Atmospheric Chem. Phys., 14, 6867–6879, https://doi.org/10.5194/acp-14-6867-2014, 2014.

Yin, Z., Cao, B., Wang, H.: Dominant patterns of summer ozone pollution in eastern China and associated atmospheric circulations, Atmospheric Chem. Phys., 19, 13933–13943, https://doi.org/10.5194/acp-19-13933-2019, 2019.

Ying, M., Zhang, W., Yu, H., Lu, X., Feng, J., Fan, Y., Zhu, Y., Chen, D.: An Overview of the China Meteorological Administration Tropical Cyclone Database, J. Atmospheric Ocean. Technol., 31, 287–301, https://doi.org/10.1175/JTECH-D-12-00119.1, 2014.

Zhan, C., & Xie, M.: Exploring the link between ozone pollution and stratospheric intrusion under the influence of tropical cyclone Ampil, Sci. Total Environ., 828, 154261, https://doi.org/10.1016/j.scitotenv.2022.154261, 2022.

Zhan, C., Xie, M., Huang, C., Liu, J., Wang, T., Xu, M., Ma, C., Yu, J., Jiao, Y., Li, M., Li, S., Zhuang, B., Zhao, M., & Nie, D.: Ozone affected by a succession of four landfall typhoons in the Yangtze River Delta, China: Major processes and health impacts, Atmospheric Chem. Phys., 20(22), 13781–13799, https://doi.org/10.5194/acp-20-13781-2020, 2020.

Zhang, J., Gao, Y., Luo, K., Leung, L.R., Zhang, Y., Wang, K., Fan, J.: Impacts of compound extreme weather events on ozone in the present and future, Atmospheric Chem. Phys., 18, 9861–9877, https://doi.org/10.5194/acp-18-9861-2018, 2018.

Zhang, M., Yang, Y., Zhan, C., Zong, L., Gul, C., & Wang, M.: Tropical cyclone-related heatwave episodes in the Greater Bay Area, China: Synoptic patterns and urban-rural disparities. Weather and Climate Extremes, 44, 100656. https://doi.org/10.1016/j.wace.2024.100656, 2024.

728   Zhang, Y., Dai, J., Li, Q., Chen, T., Mu, J., Brasseur, G., Wang, T., Xue, L.: Biogenic volatile organic

729   compounds enhance ozone production and complicate control efforts: Insights from long-term

730   observations   in   Hong   Kong,   Atmos.   Environ.,   309,   119917,

731   https://doi.org/10.1016/j.atmosenv.2023.119917, 2023.

732   Zhou, Y., Yang, Y., Wang, H., Wang, J., Li, M., Li, H., Wang, P., Zhu, J., Li, K., Liao, H.: Summer

733   ozone pollution in China affected by the intensity of Asian monsoon systems, Sci. Total

734   Environ., 849, 157785, https://doi.org/10.1016/j.scitotenv.2022.157785, 2022.

735

736 **Table 1.** Observed and simulated averaged surface MDA8 ozone ($\mu g/m^3$) in the Yangtze River Delta

737 (YRD, 118-122° E, 30-33° N) and the Pearl River Delta (PRD, 110-115.5° E, 21.5-24° N) during

738 TC-HDs and AHDs, as well as their differences (TC-HDs minus AHDs).

	YRD		PRD	
	Observed	Simulated	Observed	Simulated
TC-HDs	134.71	177.17	97.93	123.91
AHDs	147.92	199.11	91.13	116.91
Differences	−13.21	−21.94	6.8	7

739

740 **Table 2.** Contributions of difference processes for the anomalous ozone mass (Gg O_3/day) from

741 surface to 500 hPa for TC-HDs and AHDs relative to the summer climatology and their difference

742 (TC-HDs minus AHDs) for YRD.

	Net chemical production	Vertical advection	Horizontal advection	Mixing
TC-HDs	1.70	0.03	−2.18	0.004
AHDs	0.46	−0.04	−1.03	−0.12
Differences	1.24	0.07	−1.15	0.12

743

744

745

746   **Table 3.** Contributions of difference processes for the anomalous ozone mass (Gg O_3/day) from

747   surface to 500 hPa for TC-HDs and AHDs relative to the summer climatology and their difference

748   (TC-HDs minus AHDs) for PRD.

	Net chemical production	Vertical advection	Horizontal advection	Mixing
TC-HDs	0.21	−0.13	0.97	−0.002
AHDs	0.06	0.09	−0.84	−0.05
Differences	0.15	−0.22	1.81	0.05

749

750
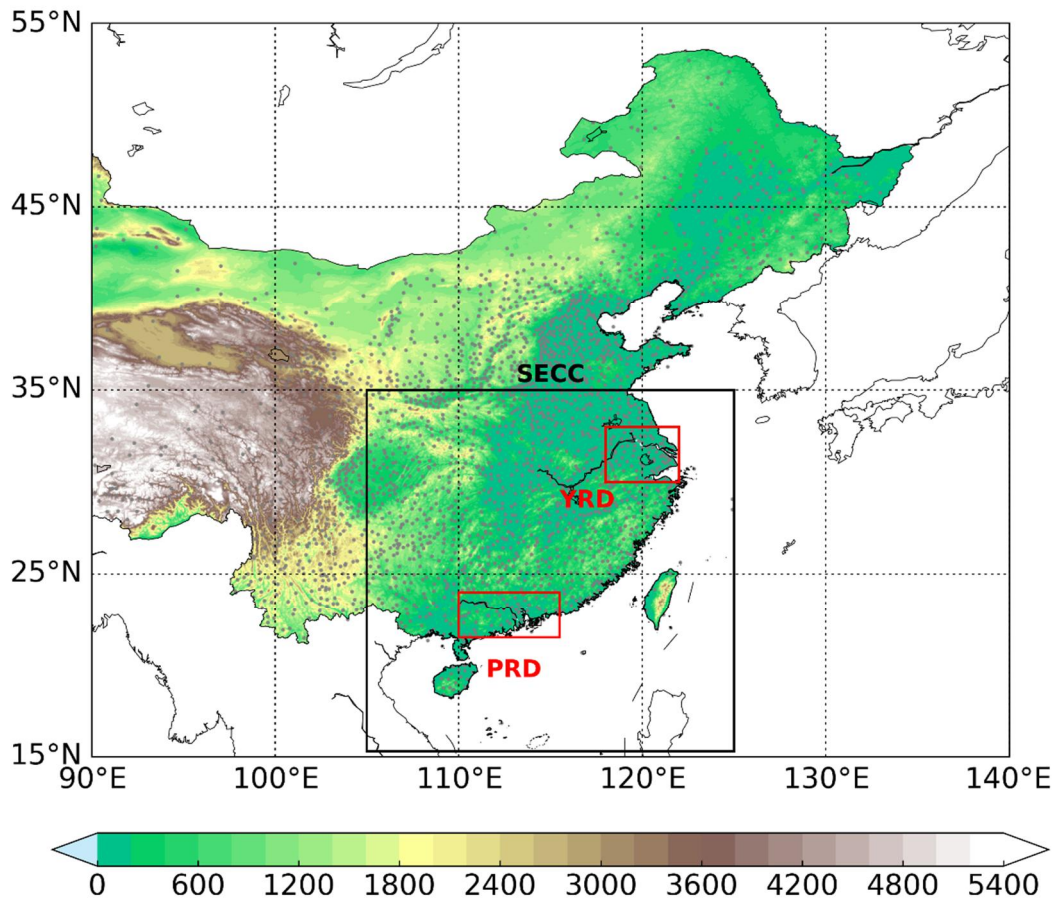
Figure 1. Topographic map of China with SECC (black box) and megacity clusters YRD and PRD outlined (red boxes). Gray points represent the temperature observation stations.

756
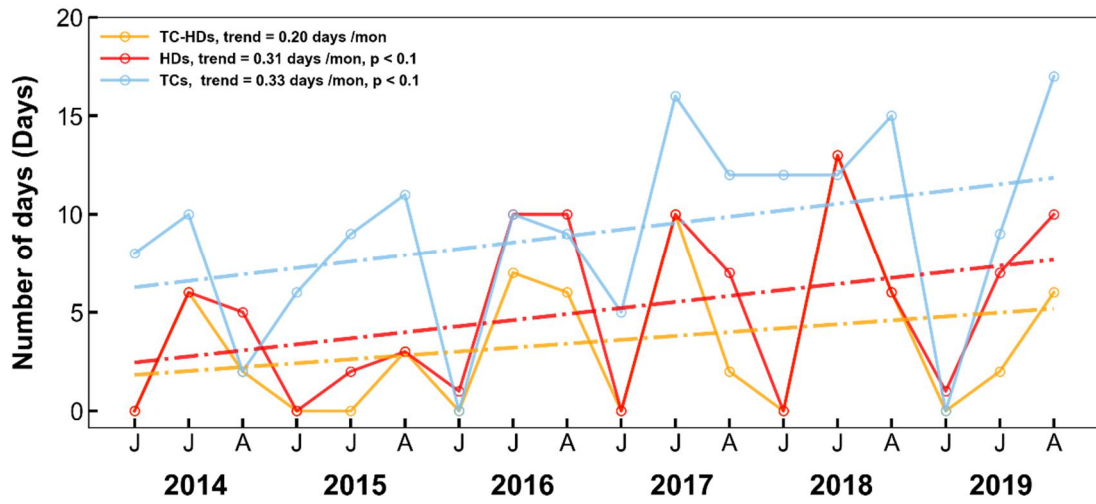
Figure 2. Monthly variations of the number of days of TC-HDs, total HDs, and total TCs during the

758 summer season (June, July and August) from 2014-2019.

759

760
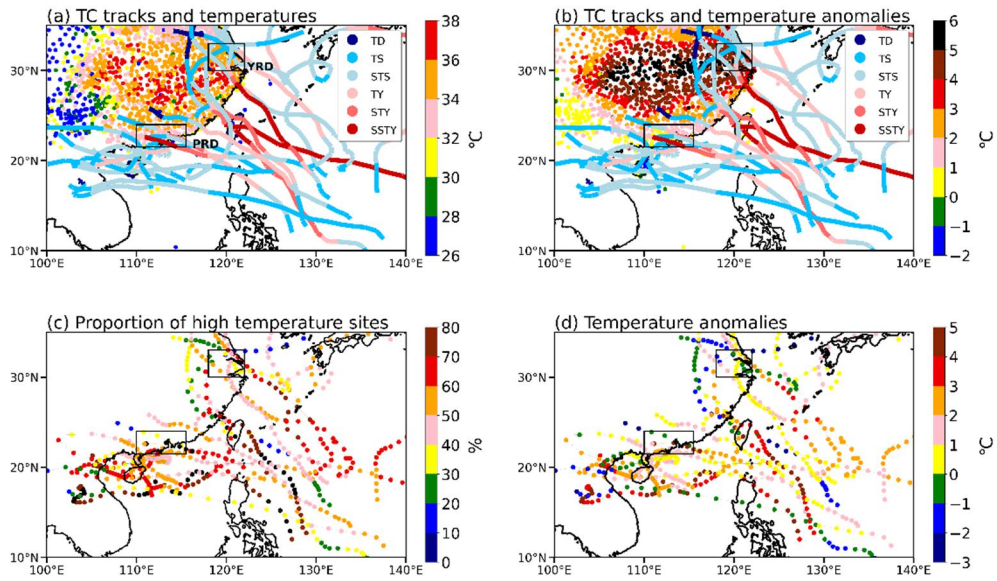
Figure 3. (a) The distribution of average Tmax (dots) and TC tracks during TC-HDs. (b) The Area

average of Tmax anomalies during TC-HDs period relative to the summer climatology (June to

August of 2014-2019), along with the TC tracks categorized by different intensities. (c) The

proportion of high-temperature sites (Tmax $\geqslant$ 35°C) over land region of SECC along with the

movements of the TCs. The proportion of high-temperature sites refers to the percentage of high-

temperature sites within all stations in the SECC region. (d) The average of Tmax anomalies for all

observational sites within SECC relative to the summer climatology, along with the movements of

TCs. YRD and PRD regions are outlined in black boxes in each panel.

769
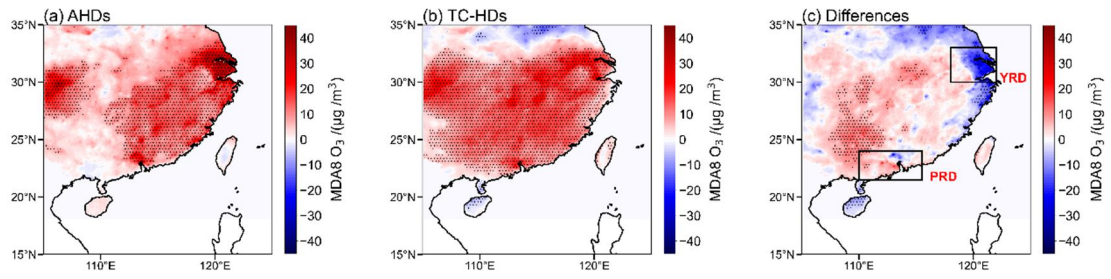
Figure 4. The spatial distribution of surface MDA8 ozone concentration anomalies during the periods of (a) AHDs, (b) TC-HDs relative to the summertime climatology, as well as (c) their differences (TC-HDs minus AHDs). Stippling regions indicate ozone anomalies that are significantly difference from zero at the 95% confidence level. YRD and PRD regions are outlined in black boxes in panel c.
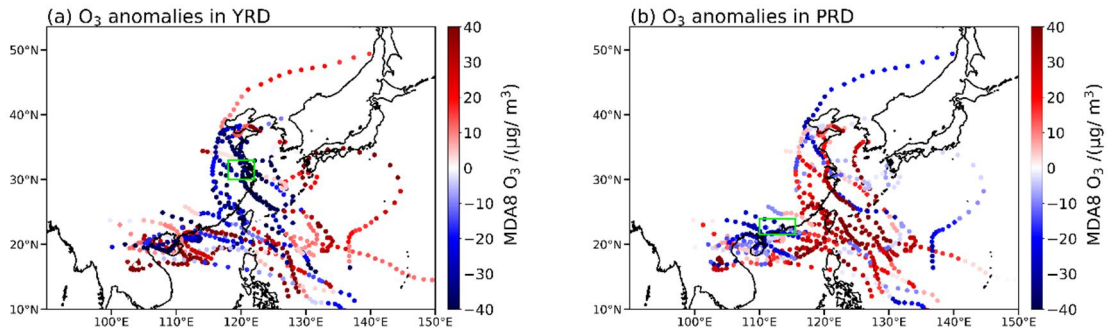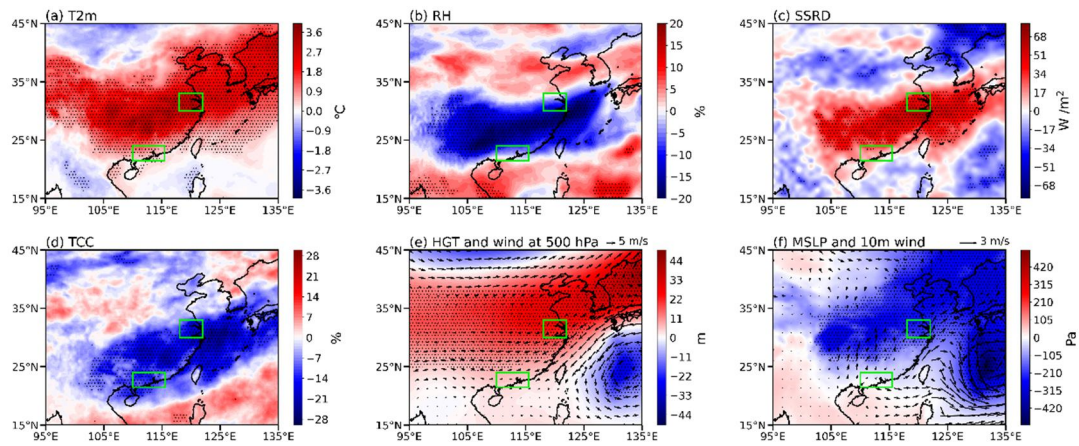
777

778 **Figure 5.** The average anomalies of surface MDA8 ozone concentrations over land regions of SECC

779 along with the movements of TCs associated with TC-HDs for (a) YRD and (b) PRD regions. YRD

780 (a) and PRD (b) regions are outlined in green boxes in panel (a) or (b).

781

Figure 6. The spatial distribution for the composites anomalies of (a) air temperature at 2m (T2m),

(b) relative humidity (RH), (c) surface solar radiation downwards (SSRD), (d) total cloud cover

(TCC), (e) geopotential height (HGT) and winds at 500hPa, and (f) mean surface level pressure

(MSLP) and 10-meter winds during AHDs relative to the summer climatology. Stippling indicates

statistically significant anomalies above 95% confidence level. YRD and PRD regions are outlined

in green boxes in each panel.
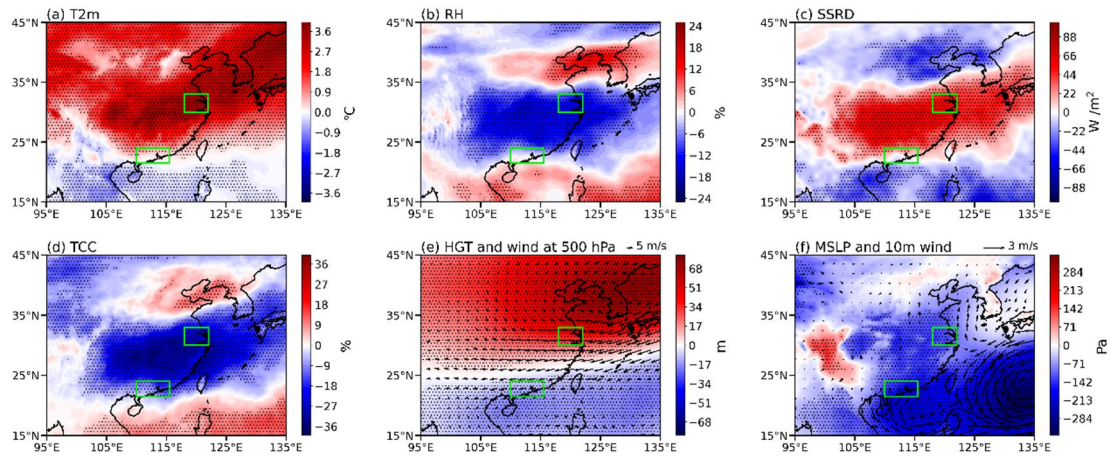
790

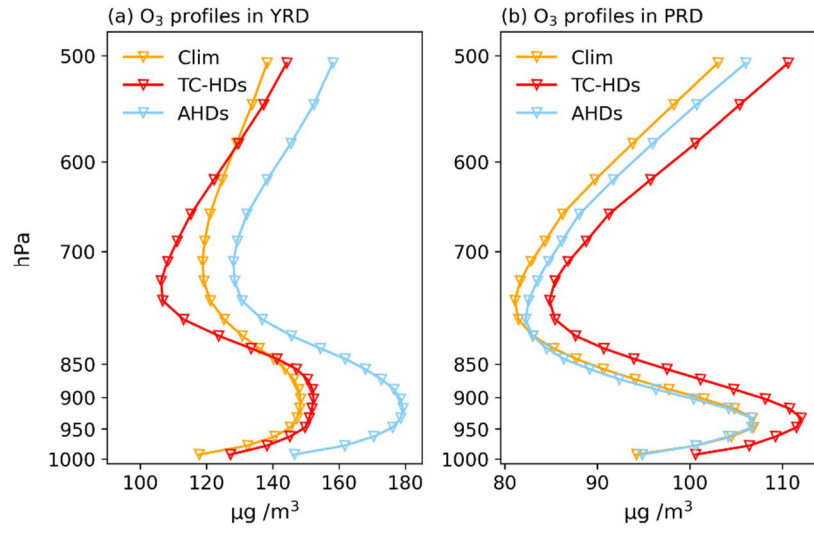791 **Figure 7.** Same as in Figure 6, but for the anomalous meteorological conditions during TC-HDs.

792
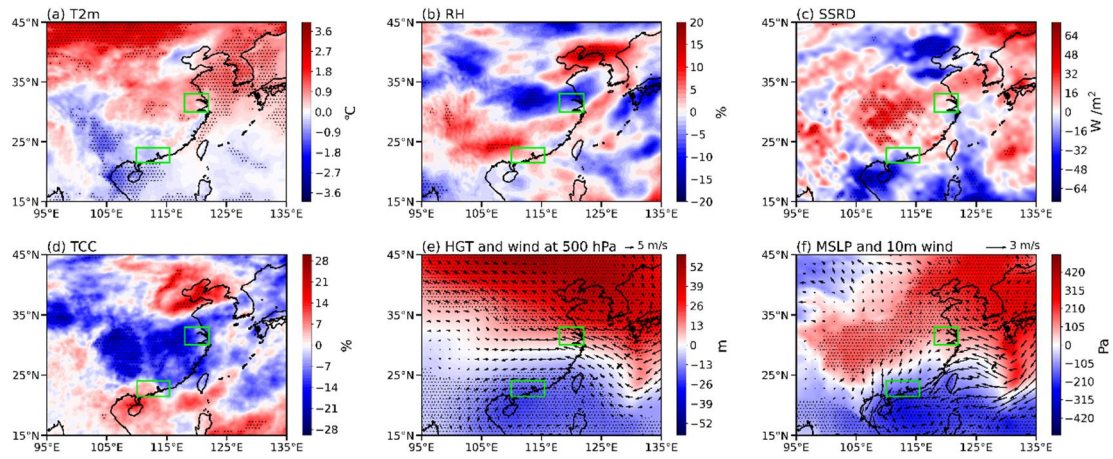
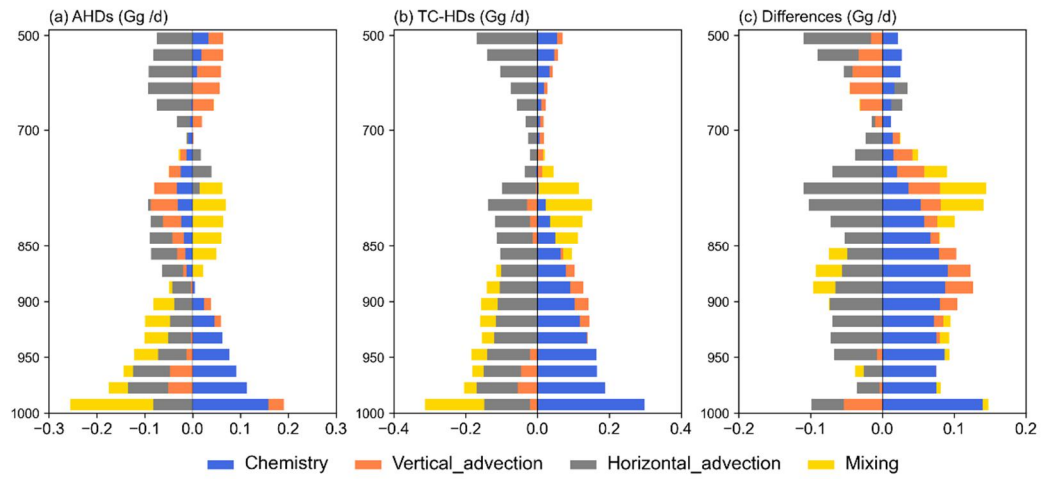**Figure 8.** Same as in Figure 6, but for the differences between TC-HDs and AHDs (TC-HDs minus AHDs).

797

Figure 9. Vertical profiles of simulated daily ozone concentrations (μg/m³) averaged over land

799   regions of SECC for TC-HDs, AHDs and for the summertime climatology (Clim) during 2014-2019
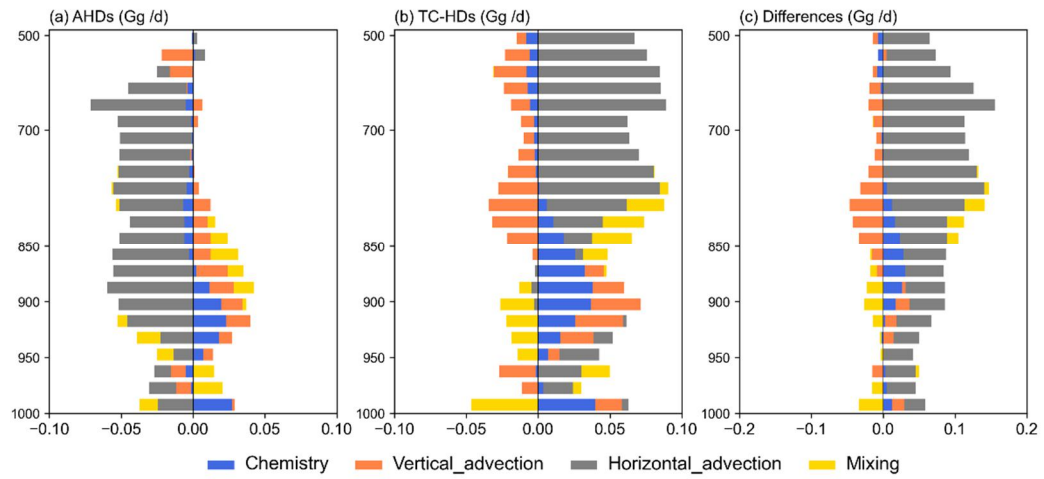
800   for (a) YRD and (b) PRD.

801

Figure 10. Vertical profiles of net changes in ozone mass (Gg O_3/day) anomalies averaged for YRD for each process during (a) AHDs, (b) TC-HDs relative to summertime climatology, and their differences (TC-HDs minus AHDs).

807

Figure 11. Same as in Figure 10, but for the vertical profiles of net changes in ozone mass (Gg

809 O_3/day) anomalies averaged for PRD for each process.